Available online at www.sciencedirect.com
ScienceDirect
Tetrahedron
Tetrahedron 63 (2007) 12429–12436

Columnar mesophases and phase behaviors of novel polycatenar mesogens containing bi-1,3,4-oxadiazole

Songnan Qu and Min Li*

Key Laboratory of Automobile Materials (Jilin University), Ministry of Education, Institute of Materials Science and Engineering, 10 Qianwei road, Jilin University, Changchun 130012, PR China

Received 22 July 2007; revised 12 September 2007; accepted 14 September 2007
Available online 22 September 2007

Abstract—A new series of liquid-crystalline bi-1,3,4-oxadiazole derivatives (2,2′-bis(3,4,5-trialkoxyphenyl)-bi-1,3,4-oxadiazole, BOXD-T*n*, *n*=3, 4, 5, 6, 7, 8, 10, 14) were designed and synthesized. They have been confirmed to give rise to columnar mesophases. The columnar mesophases for BOXD-T*n* (*n*=5, 6, 7, 8, 10) could be supercooled to −20 °C on the cooling runs. A room temperature Col_{ho} phase was obtained for BOXD-T14. All BOXD-T*n* exhibit good fluorescence properties either in cyclohexane or in solid state.

1. Introduction

Organic semiconducting materials with high carrier mobilities are desirable for various electronic applications including light-emitting diodes, solar cells, and field-effect transistors. However, most of the organic compounds known for optoelectronic applications still present some major limitations such as low electron conductivity and/or low luminescence efficiency. 1,3,4-Oxadiazoles derivatives have enjoyed widespread use as electron-transporting/hole blocking (ETHB) materials, emitting layers in electroluminescent diodes or for non-linear optical process, due to the electron-deficient nature of the heterocycle, high photoluminescence quantum yield, and good thermal, and chemical stabilities.[1] Non-mesomorphic 2,5-bis(4-naphthyl)-1,3,4-oxadiazole[2] has been demonstrated as one of the best organic electron conductors, and several oxadiazole-based compounds have been recently used as electron transport materials in organic light-emitting diodes (OLEDs).[3]

Liquid-crystalline materials, which present self-organizing ability, fluidity, and the ease of defect-free orientation with special treatment, have been recently recognized to have great advantages in manipulation of optimized high-efficiency organic electro-optic devices.[4] Materials with columnar mesophases in which molecules self-assemble to columnar structures have attracted increasing attention because the overlapping of π-orbitals results in one-dimensional semiconductors with a better performance than conjugated polymers.[5] Most of the reported mesomorphic 1,3,4-oxadiazole derivatives were generally rod-like molecules[6] exhibiting nematic/smectic phase. For example, 2,5-hexyloxybiphenyl-hexyloxyphenyl-oxadiazole (HOBP-OXD) exhibited smectic phases and high electron mobility (over 10^{-3} $cm^2/V/s$) was found in its high-ordered smectic phase.[6d] In contrast, columnar 1,3,4-oxadiazole derivatives were relatively limited. A star-shaped discotic molecule containing 1,3,5-triethynylbenzene and oxadiazole-based rigid arms was reported to exhibit a discotic nematic phase (N_{Col}).[7] Marder et al. reported that discotic molecules with benzene or triazine cores and three (trialkoxyaryl) oxadiazole arms exhibited columnar mesophases and demonstrated that these materials may find applications in organic electronics.[8] Lai et al. reported that 2,5-bis(3,4,5-trialkoxy phenyl)-1,3,4-oxadiazoles exhibited hexagonal columnar phases (Col_h), while their complexes with metals, Col_r and Col_h.[9]

Our present work aimed at developing new liquid-crystalline 1,3,4-oxadiazole derivatives, e.g., 2,2′-bis(3,4,5-trialkoxyphenyl)-bi-1,3,4-oxadiazole, BOXD-T*n*, *n*=3, 4, 5, 6, 7, 8, 10, 14. They have been confirmed to give rise to columnar mesophases. The columnar mesophases of BOXD-T*n* (n=5, 6, 7, 8, 10) could be supercooled to low temperature (−20 °C) due to their slow crystallization. A room temperature ordered columnar phase was identified for BOXD-T14. All the compounds exhibit good fluorescence properties either in cyclohexane or in bulk.

Keywords: 1,3,4-Oxadiazole; Liquid crystals; Columnar mesophases; Fluorescence.
* Corresponding author. Tel.: +86 431 85168254; e-mail: minli@mail.jlu.edu.cn

0040–4020/$ - see front matter © 2007 Elsevier Ltd. All rights reserved.
doi:10.1016/j.tet.2007.09.028

2. Results and discussion

2.1. Synthesis

Ethyl 3,4,5-trihydroxy benzoate, oxalyl chloride, and 1-bromide alkane were used as received. 3,4,5-Trialkoxy-benzoyl hydrazines **2** were prepared according to the literature.[8] Tetrahydrofuran (THF) was refluxed over sodium under argon and distilled before use. Scheme 1 shows the synthetic route for BOXD-T*n*. Anhydrous K_2CO_3 (30 g) and ethyl 3,4,5-trihydroxy benzoate (5.4 mmol) were added to a deoxygenated mixture of DMF (100 mL) and of 1-bromide alkane (18.1 mmol) under nitrogen. The mixture was heated at 80 °C for 6 h. The reaction mixture was cooled to room temperature, water (500 mL) was added, and the product was extracted with diethyl ether. The extractive solution was washed with water and dried over $MgSO_4$. After filtration, the solvent was evaporated under reduced pressure, and the crude product was purified through a column of silica gel using 2% ethyl acetate in hexane as eluent to afford **1**. A solution of **1** (19.2 mmol) and excess hydrazine monohydrate in ethanol (180 mL) was refluxed for 40 h. Water (100 mL) was added and the resulting precipitate was collected, dried under vacuum, and recrystallized from ethanol/water to give pure **2**. Oxalyl chloride (11.2 mmol) was regularly injected into the THF solution of 3,4,5-trialkoxy-benzoyl hydrazine **2** (23.1 mmol) under vigorous stirring at room temperature for 8 h. The resulted products of oxalyl acid *N*′,*N*′-di(3,4,5-trialkoxylbenzoyl)-hydrazide **3** were purified by recrystallizing from alcohol. The purified **3** was dissolved in phosphorous oxychloride ($POCl_3$) and refluxed for about 40 h. Excess $POCl_3$ was removed through distillation and the residue was slowly added into icewater. After the removal of solvent under reduced pressure, the crude products were further purified through a column of silica gel using 2% ethyl acetate in chloroform as eluent to afford BOXD-T*n*.

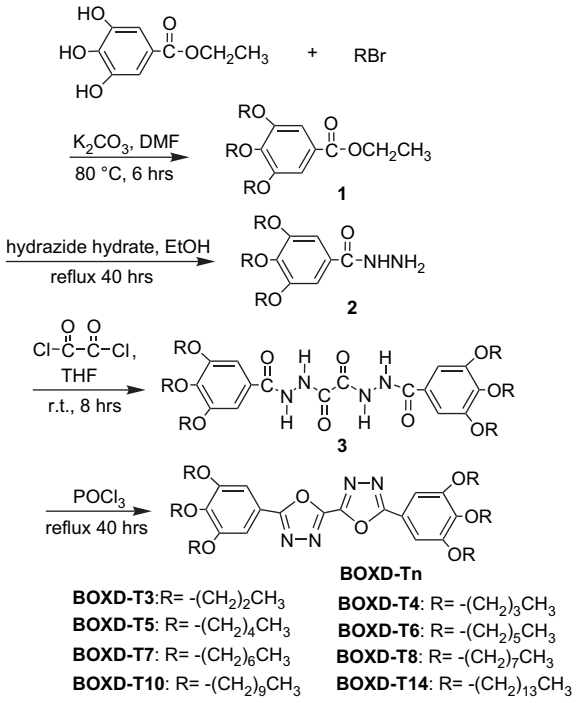

Scheme 1. Synthesis of BOXD-T*n*.

2.2. Mesomorphic properties

The phase transition temperatures and transition enthalpies for BOXD-T*n* (*n*=3, 4, 5, 6, 7, 8, 10, 14) are summarized in Table 1. It can be seen that the mesophase behaviors are greatly affected by the length of the terminal chains. BOXD-T3 and BOXD-T4 are non-mesomorphic perhaps due to the shorter terminal alkoxy groups, which cause the higher melting point and thus suppress the LC phase. On the other hand, BOXD-T*n* (*n*=5, 6, 7, 8, 10, 14) with longer alkoxyl terminal groups exhibited columnar phases as confirmed by polarizing microscopy, calorimetry, and X-ray diffraction investigations.

Figures 1 and 2 show the DSC thermograms of BOXD-T*n* (*n*=5, 6, 7, 8, 10, 14) on the first heating and cooling runs at a scanning rate of 10 °C/min. BOXD-T5 exhibited monotropic mesophases, while others with longer terminal chains exhibited enantiotropic mesophases. It should be mentioned that no crystallization was observed for BOXD-T*n* (*n*=5, 6, 7, 8, 10, 14) even when they were cooled to −20 °C at cooling rate of 10 °C/min. On subsequent heating (10 °C/min), the phase transition sequences of BOXD-T*n* (*n*=6, 7, 8, 10, 14) were reversible, while complex thermal behaviors were observed for BOXD-T5 (Fig. 3). Upon heating BOXD-T5 at 10 °C/min, an exothermic process between 56 °C and 74 °C, which was partially overlapped with the endothermic peak centered at 67.8 °C, followed by an endothermic peak centered at 77.1 °C (13.8 kJ/mol) was observed (Fig. 3f). In contrast, this exothermic process shifted to lower temperature, e.g., between 47 °C and 63 °C with the heat of 26.19 kJ/mol at 2 °C/min and the high-temperature endothermic peak centered at 74.7 °C (36.36 kJ/mol), which was assigned to the crystalline–isotropic transition similar to that in its first heating run (Fig. 3g), indicating that crystallization of BOXD-T5 took place during heating the mesophase. The lower the heating rates, the lower the crystallization temperature and the higher the enthalpic changes, suggesting its kinetic-controlled feature of the crystallization. The endothermic peak at 67 °C corresponding to mesophase to isotropic transition

Table 1. Phase transition temperatures (T/°C) and enthalpies (Δ*H*/kJ/mol in brackets) of BOXD-T*n* (*n*=3, 4, 5, 6, 7, 8, 10, 14) on the first heating and cooling runs[a]

Compound	Heating		Cooling	
BOXD-T3	Cr–I	182.3 (38.9)	I–Cr	175.9 (37.8)
BOXD-T4	Cr–I	139.8 (43.9)	I–Cr	122.8 (42.9)
BOXD-T5			Col_r–Col_L	23.2 (0.74)
	Cr–I	76.7 (39.4)	I–Col_L	63.8 (4.23)
BOXD-T6	Cr–Col_L	69.0 (50.8)	Col_L–Col_r	9.0 (0.3)
	Col_L–I	73.2 (3.8)	I–Col_L	70.8 (3.8)
BOXD-T7	Cr–Col_L	67.3 (54.2)		
	Col_L–I	77.7 (4.9)	I–Col_L	76.1 (4.5)
BOXD-T8	Cr–Col_L	67.3 (57.1)		
	Col_L–I	83.5 (4.4)	I–Col_L	81.1 (4.2)
BOXD-T10	Cr1–Cr2	36.4 (5.8)		
	Cr2–Col_L	60.6 (64.9)		
	Col_L–I	83.5 (4.9)	I–Col_L	79.8 (4.8)
BOXD-T14			Col_{II}–Col_{ho}	17.3 (15.2)
			Col_I–Col_{II}	23.1 (5.6)
	Cr–Col_L	68.6 (97.3)	Col_L–Col_I	26.2 (28.9)
	Col_L–I	80.9 (5.4)	I–Col_L	77.7 (5.3)

[a] Scanning rate of 10 °C/min.

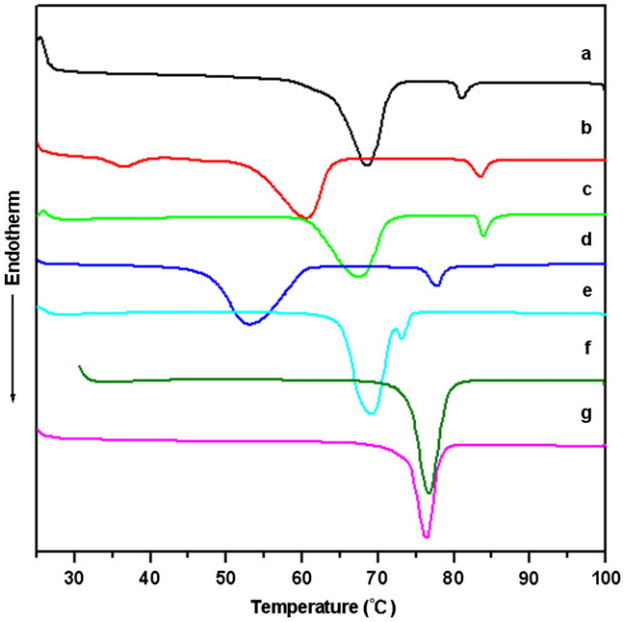

Figure 1. DSC curves of (a) BOXD-T14, (b) BOXD-T10, (c) BOXD-T8, (d) BOXD-T7, (e) BOXD-T6, (f) BOXD-T5 on the first heating run, and (g) BOXD-T5 measured after cooling from its isotropic state and holding at room temperature for 48 h (heating rate: 10 °C/min).

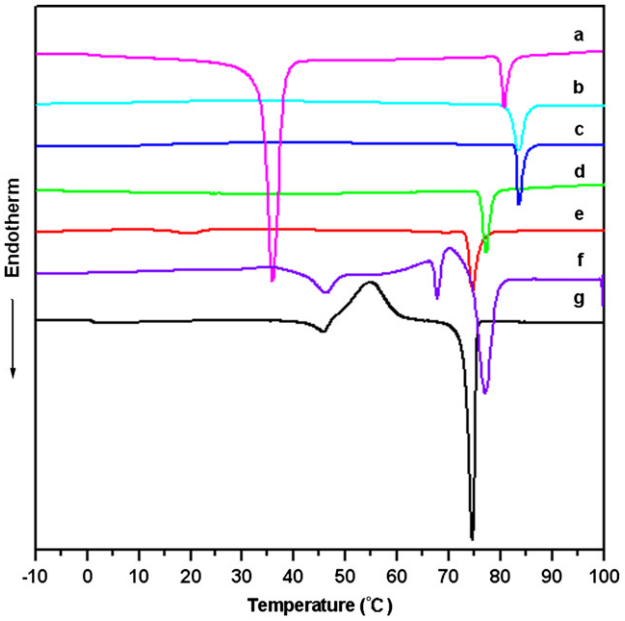

Figure 3. DSC curves of (a) BOXD-T14, (b) BOXD-T10, (c) BOXD-T8, (d) BOXD-T7, (e) BOXD-T6, and (f) BOXD-T5 on the subsequent heating run (heating rate: 10 °C/min), and (g) BOXD-T5 on the subsequent heating run (heating rate: 2 °C/min).

was not detected for 2 °C/min due to the complete crystallization, thus only melting of the crystals was observed. The heating curve of BOXD-T5 annealed at room temperature for three days, is almost the same as its first heating curve (Fig. 1g). Similar behavior was also observed in BOXD-T*n* (*n*=6, 7, 8, 10), indicating their slow and kinetic-controlled feature of crystallization.

Figure 4a shows the optical textures of BOXD-T5 in its mesophase on the cooling run (10 °C/min). The focal-conic texture typical of columnar phases (Col) was observed on slowly cooling from the isotropic liquid and the black areas were homeotropic domains. The XRD pattern in this columnar phase of BOXD-T5 (Fig. 5a) consisted of one strong (100) (*d*=21.4 Å) peak, two weak (200) (*d*=10.6 Å) and (300) (*d*=7.0 Å) peaks in the small angle regions as well as a diffuse halo centered at 4.5 Å, suggesting a lamellar structure. Thus this phase was identified as Col_L. Similar mesophases were observed in other BOXD-T*n* (*n*=6, 7, 8, 10, 14) during cooling from their isotropic states. Upon further cooling the Col_L phase of BXOD-T5, a new phase developed without obvious morphology changes. The XRD pattern in this phase of BOXD-T5 consists of two strong peaks at 22.4 Å (200), 20.4 Å (110) and five weak peaks at 11.0 Å (400), 9.9 Å (220), 6.6 Å (330), 5.5 Å (800), 4.9 Å (440), which correspond to a rectangular columnar packing (Col_r) (Fig. 5b). Similar sequence was observed in BOXD-T6. The XRD results of BOXD-T*n* (*n*=5, 6, 7, 8, 10, 14) in their columnar phases are listed in Table 2.

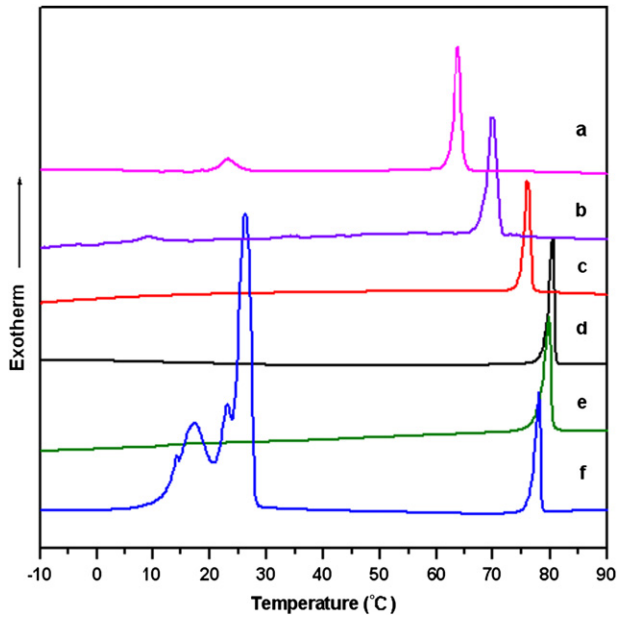

Figure 2. DSC curves of (a) BOXD-T5, (b) BOXD-T6, (c) BOXD-T7, (d) BOXD-T8, (e) BOXD-T10, and (f) BOXD-T14 on the cooling runs (cooling rate: 10 °C/min).

On the subsequent heating of BOXD-T5, crystallization process was observed under POM. Figure 4b showed the pin-like textures, which developed from the pseudo focal-conic textures at 60 °C at a heating rate of 10 °C/min. Figure 6c showed the morphology of BOXD-T5 at 60 °C at heating rate of 2 °C/min, suggesting that the percentage of crystallization was bigger at lower heating rate, which was consistent with that of the DSC results. Crystallization of BOXD-T5 during heating was also further confirmed by XRD. The XRD pattern (Fig. 5c) for BOXD-T5 at 65 °C on subsequent heating (2 °C/min) consisted of two strong peaks in low-angle region and several weak peaks in both low- and high-angle regions, indicating the formation of a crystalline phase. Crystallization was observed for the annealed BOXD-T5 at room temperature for more than 3 days under POM (Fig. 5d). Similar phenomena was also observed in other BOXD-T*n* (*n*=6, 7, 8, 10).

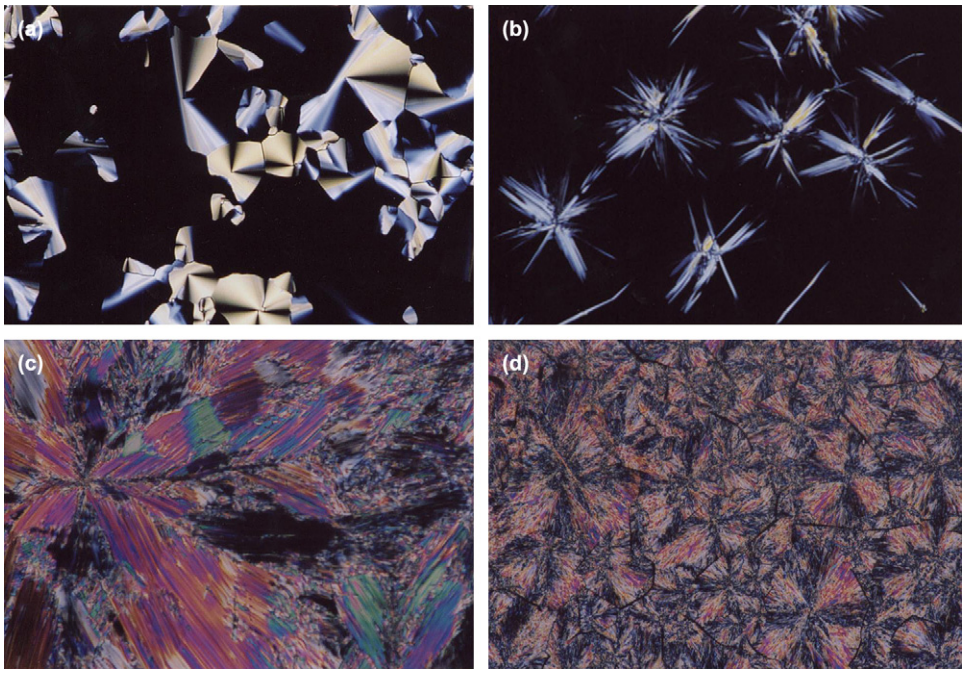

Figure 4. Optical textures observed for BOXD-T5 at (a) 40 °C (×200) on the cooling run, (b) 60 °C (×200) on the subsequent heating (10 °C/min), (c) 60 °C (×200) on the subsequent heating (2 °C/min), and (d) holding for 3 days at room temperature (×200).

On the cooling run (10 °C/min), BOXD-T14 exhibited polymesomorphic phase sequence (Fig. 2f). An exothermic peak centered at 26.2 °C (28.9 kJ/mol) was followed by two exothermic peaks centered at 23.1 °C (5.6 kJ/mol) and 17.3 °C (15.2 kJ/mol), respectively. As the three exothermic peaks are so close and partially overlapped, we have not got

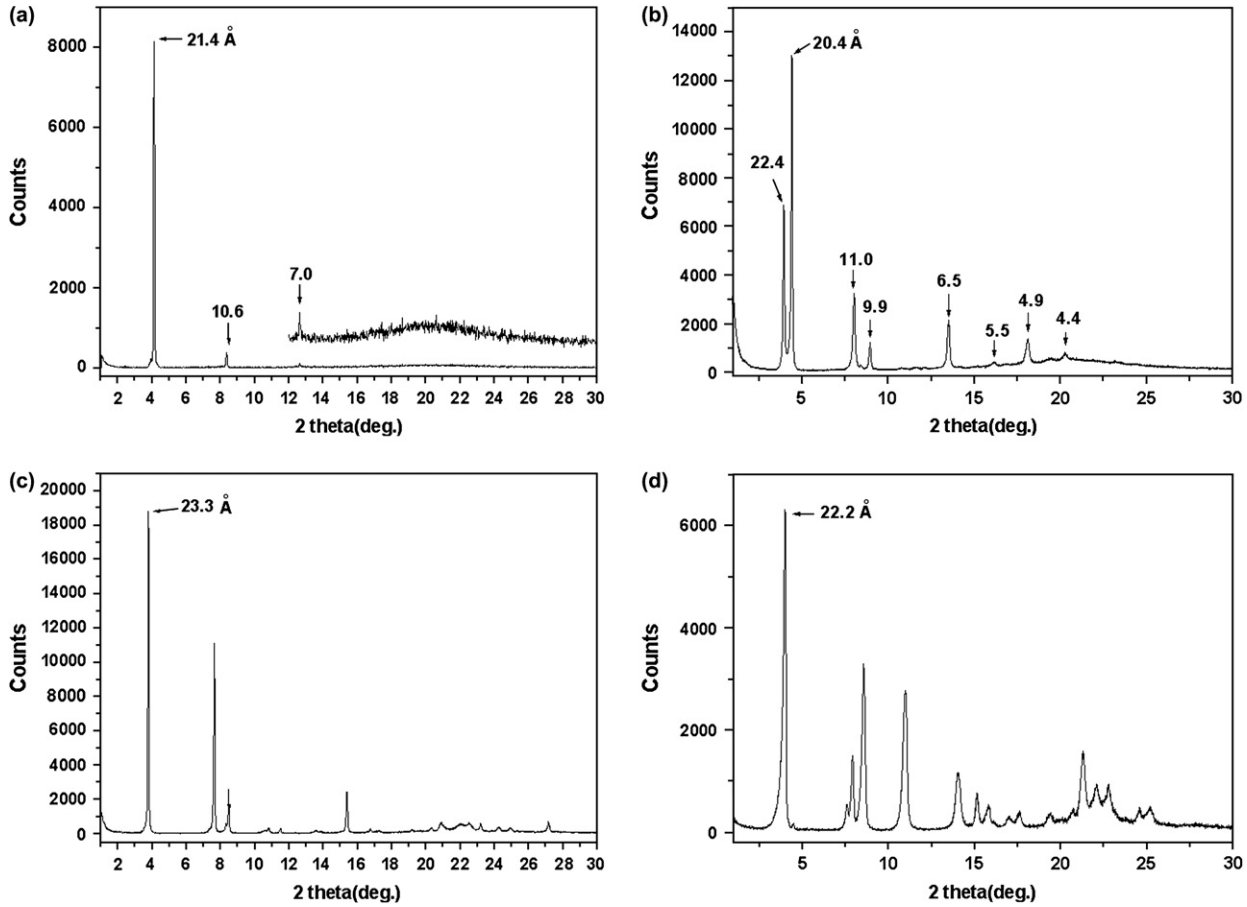

Figure 5. X-ray diffraction patterns of BOXD-T5 (a) at 40 °C and (b) at 20 °C on the first cooling run (10 °C/min), (c) at 60 °C on subsequent heating run (2 °C/min), and (d) holding for more than 2 days at room temperature.

Table 2. Powder WAXD results of BOXD-Tn in their mesophases

Compound	Mesophase	*hkl*	*d*, obsd (Å)	*d*, calcd (Å)	Lattice parameter (Å)
BOXD-T5	Col_r (20 °C)	200	22.4	22.2	*a*=44.4
		110	20.4	20.2	*b*=22.7
		400	11.0	11.1	
		220	9.9	10.1	
		330	6.6	6.7	
		800	5.5	5.6	
		440	4.9	5.0	
		350	4.4	4.3	
			4.4 (halo)		
	Col_L (40 °C)	100	21.4	21.4	
		200	10.6	10.7	
			4.4 (halo)		
BXOD-T6	Col_r (5 °C)	200	23.9	23.9	*a*=47.8
		110	21.6	21.4	*b*=24.0
		400	11.8	12.0	
		220	10.6	10.7	
		330	7.0	7.1	
		800	5.8	5.8	
		440	5.2	5.3	
			4.4 (halo)		
	Col_L (60 °C)	100	22.5	22.5	
		200	11.1	11.3	
		300	7.4	7.5	
			4.4 (halo)		
BOXD-T7	Col_L (35 °C)	100	23.8	23.8	
		200	11.8	11.9	
		300	7.8	7.9	
		400	5.8	5.8	
			4.4 (halo)		
BOXD-T8	Col_L (35 °C)	100	24.3	24.4	
		200	12.2	12.2	
		400	6.1	6.1	
			4.4 (halo)		
BOXD-T10	Col_L (35 °C)	100	26.8	26.8	
		200	13.4	13.4	
			4.5 (halo)		
BOXD-T14	Col_L (35 °C)	100	30.4	30.4	
		200	15.0	15.2	
			4.5 (halo)		
	Col_{ho} (10 °C)	100	30.8	30.8	*a*=35.6
		110	17.8	17.8	
		200	15.0	15.4	
		210	11.5	11.6	
		300	10.0	10.2	
			6.5		
		001	4.2	4.2	
			4.4 (halo)		

further experimental evidence to identify their structures. At this stage, we named the two as Col_I and Col_{II}, respectively. On further cooling, another stable high-ordered columnar mesophase developed. Figure 6 shows the optical textures of BOXD-T14 at 10 °C. The XRD pattern of this columnar phase of BOXD-T14 is shown in Figure 7b. In the low-angle region, a diffraction pattern of one strong peak at 30.8 Å (100) and five weak peaks at 17.8 Å (110), 15.0 Å (200), 11.5 Å (210), 10.0 Å (300) corresponded to a hexagonal arrangement. In the high-angle region, a diffuse halo centered at 4.4 Å confirmed its LC nature, and a relatively strong peak at 4.2 Å, which is assigned to (001) reflection, indicated a certain degree of order along the columns. Thus, it was identified as Col_{ho} phase, which was stable at room temperature, and no crystallization was observed even after more than three weeks.

2.3. Optical properties

The UV–vis absorption and photoluminescence spectra for BOXD-T4 in cyclohexane are presented in Figure 8. The photophysical properties of BOXD-T*n* in cyclohexane (10^{-5} mol/L) are summarized in S-Table 1. The absorption spectra of BOXD-T*n*, in which an intense broad absorption at 329 nm was observed, were similar in shape because of their structural similarities. The PL spectra of BOXD-T*n* were recorded in cyclohexane at $\lambda_{exc.}$=340 nm. All the compounds exhibit strong fluorescence with two maxima at 378 and 395 nm. Fluorescence quantum yields were determined relative to quinine sulfate in sulfuric acid aqueous solution (Φ_F=0.546) and calculated according to literature.[10] All the compounds exhibited high quantum yield (Φ_F>90%) in cyclohexane (10^{-5} mol/L).

Figure 6. Optical textures observed for BOXD-T14 at (a) 10 °C (×200) on the cooling run.

In addition, all BOXD-T*n* exhibited strong fluorescence in bulk. Figure 9 shows the PL spectra of BOXD-T*n* (*n*=5, 6, 7, 8, 10, 14) in their mesophases (cooling rate 10 °C/min) at room temperature. The maximum emissions centered at 426 nm for BOXD-T5, 438 nm for BOXD-T6, 448 nm for BOXD-T7, 433 nm for BOXD-T8, 434 nm for BOXD-T10, and 426 nm for BOXD-T14.

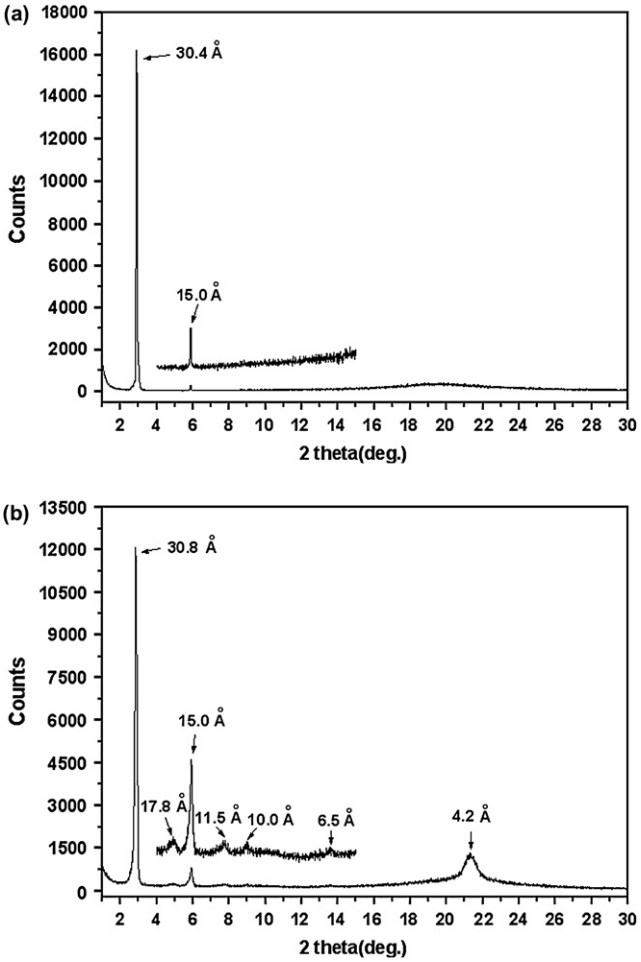

Figure 7. X-ray diffraction patterns of BOXD-T14 (a) at 65 °C and (b) at 10 °C on the first cooling run (10 °C/min).

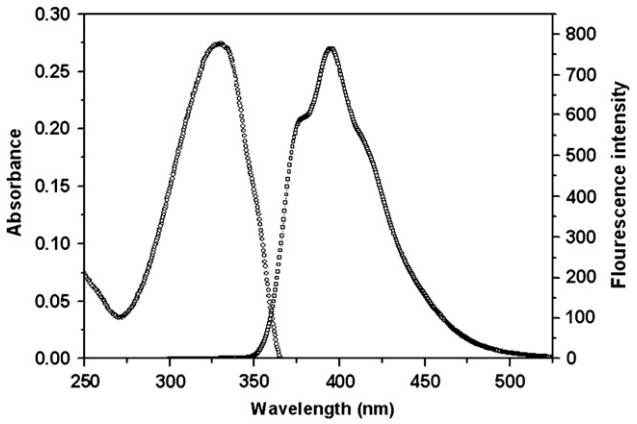

Figure 8. UV–vis (○) and PL spectra (□) of BOXD-T4 in cyclohexane (1×10^{-5} mol/L) at room temperature.

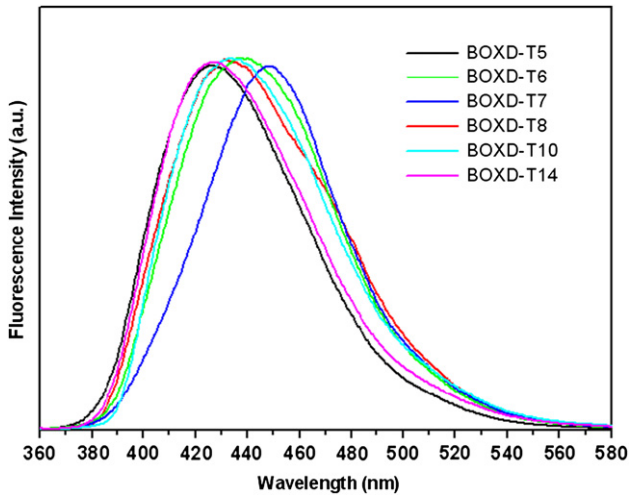

Figure 9. Corrected PL spectra of BOXD-T*n* (*n*=5, 6, 7, 8, 10, 14) in their mesophases (cooling rate 10 °C/min) at room temperature. Spectra are normalized to the same height at the maximum.

3. Conclusions

A new series of liquid-crystalline bi-1,3,4-oxadiazole derivatives (2,2′-bis(3,4,5-trialkoxyphenyl)-bi-1,3,4-oxadiazole, BOXD-T*n*, *n*=3, 4, 5, 6, 7, 8, 10, 14) were designed and synthesized. The columnar mesophases for BOXD-T*n* (*n*=5, 6, 7, 8, 10) were observed even at low temperature (−20 °C) during cooling. A room temperature Col_{ho} phase was obtained for BOXD-T14. All the compounds have been demonstrated to exhibit good fluorescence properties either in cyclohexane solution or in bulk. Potential applications for these compounds, such as optoelectronic applications, are of interest and will be examined.

4. Experimental

4.1. Characterization

^{1}H NMR spectra were recorded with a Bruker Avance 500 MHz or a Varian-300 EX spectrometer, using $CDCl_3$

as solvent and tetramethylsilane (TMS) as an internal standard (δ=0.00 ppm). ^{13}C NMR spectra were recorded with a Varian-300 EX spectrometer, using $CDCl_3$ as solvent and $CDCl_3$ as an internal standard (δ=77.00 ppm). Mass spectra were obtained by MALDI-TOF mass spectrometry. FTIR spectra were recorded with a Perkin–Elmer spectrometer (Spectrum One B). The samples were pressed tablets with KBr. Phase transitional properties were investigated by differential scanning calorimeter (DSC, Mettler Star DSC 821e). Optical textures were observed under polarized optical microscope (POM, Leica DMLP) equipped with a Leitz 350 heating stage. X-ray diffraction (XRD) was carried out with a Bruker Avance D8 X-ray diffractometer.

4.1.1. Oxalyl acid *N*′,*N*′-di(3,4,5-tripropyloxybenzoyl)-hydrazide. ^{1}H NMR: (300 MHz, $CDCl_3$), (ppm, from TMS): δ=10.29 (s, 2H), 9.14 (s, 2H), 7.06 (s, 4H), 3.96 (s, 4H), 3.88 (s, 8H), 1.76 (s,12H), 1.03–1.00 (m, 18H). FTIR: ν=3255, 3152, 3074, 2965, 2938, 2878, 1719, 1686, 1631, 1584, 1547, 1468, 1428, 1386, 1338, 1300, 1219, 1261, 1219, 1113, 1060, 1000, 960, 856, 837, 790, 751, 602 cm^{-1}. Anal. Calcd (%) for $C_{34}H_{50}N_4O_{10}$: C, 60.52; H, 7.47; N, 8.30. Found C, 60.59; H, 7.54; N, 8.31.

4.1.2. Oxalyl acid *N*′,*N*′-di(3,4,5-tributyloxybenzoyl)-hydrazide. ^{1}H NMR: (300 MHz, $CDCl_3$), (ppm, from TMS): δ=10.29 (s, 2H), 9.14 (s, 2H), 7.06 (s, 4H), 3.96 (s, 4H), 3.88 (s, 8H), 1.76 (s, 12H), 1.03–1.00 (m, 18H). FTIR: ν=3255, 3152, 3074, 2965, 2938, 2878, 1719, 1686, 1631, 1584, 1547, 1468, 1428, 1386, 1338, 1300, 1219, 1261, 1219, 1113, 1060, 1000, 960, 856, 837, 790, 751, 602 cm^{-1}. Anal. Calcd (%) for $C_{40}H_{62}N_4O_{10}$: C, 63.30; H, 8.23; N, 7.38. Found: C, 63.48; H, 8.24; N, 7.56.

4.1.3. Oxalyl acid *N*′,*N*′-di(3,4,5-tripentyloxyphenyl)-hydrazide. ^{1}H NMR: (300 MHz, $CDCl_3$), (ppm, from TMS): δ=10.61 (s, 2H), 9.61 (s, 2H), 7.07 (s, 4H), 3.93–3.83 (m, 12H), 1.72–1.69 (m, 12H), 1.49–1.33 (m, 24H), 0.93–0.87 (m, 18H). FTIR: ν=3255, 3152, 3074, 2965, 2938, 2878, 1719, 1686, 1631, 1584, 1547, 1468, 1428, 1386, 1338, 1300, 1219, 1261, 1219, 1113, 1060, 1000, 960, 856, 837, 790, 751, 602 cm^{-1}. Anal. Calcd (%) for $C_{46}H_{74}N_4O_{10}$: C, 65.53; H, 8.85; N, 6.65. Found: C, 65.48; H, 8.75; N, 6.85.

4.1.4. Oxalyl acid *N*′,*N*′-di(3,4,5-trihexyloxybenzoyl)-hydrazide. ^{1}H NMR: (300 MHz, $CDCl_3$), (ppm, from TMS): δ=10.53 (s, 2H), 9.42 (s, 2H), 7.06 (s, 4H), 3.97–3.84 (m, 12H), 1.71–1.66 (m, 12H), 1.45–1.28 (m, 36H), 0.91–0.85 (m, 18H). FTIR: ν=3338, 3211, 3013, 2957, 2932, 2872, 2860, 1719, 1695, 1624, 1582, 1467, 1427, 1386, 1337, 1234, 1216, 1001, 1043, 926, 859, 750, 777, 726 cm^{-1}. Anal. Calcd (%) for $C_{52}H_{86}N_4O_{10}$: C, 67.36; H, 9.35; N, 6.04. Found: C, 67.58; H, 9.45; N, 5.79.

4.1.5. Oxalyl acid *N*′,*N*′-di(3,4,5-triheptyloxybenzoyl)-hydrazide. ^{1}H NMR: (500 MHz, $CDCl_3$), (ppm, from TMS): δ=10.15 (s, 2H), 8.90 (s, 2H), 7.03 (s, 4H), 4.03–3.94 (m, 12H), 1.81–1.71 (m, 12H), 1.50–1.42 (m, 12H), 1.35–1.30 (m, 36H), 0.89 (t, 18H, J=6.5 Hz). ^{13}C NMR (300 MHz, $CDCl_3$): δ=165.08, 155.21, 153.18, 142.05, 125.31, 105.89, 73.44, 69.17, 31.90, 31.87, 31.81, 30.36, 29.37, 29.24, 29.12, 26.05, 26.01, 25.95, 22.65, 22.62, 14.06. FTIR: ν=3214, 3016, 2956, 2928, 2871, 2857, 1693, 1629, 1580, 1468, 1428, 1384, 1336, 1234 , 1212, 1114, 1004, 857, 750, 720 cm^{-1}. Anal. Calcd (%) for $C_{58}H_{98}N_4O_{10}$: C, 68.88; H, 9.77; N, 5.54. Found: C, 69.16; H, 10.05; N, 5.47.

4.1.6. Oxalyl acid *N*′,*N*′-di(3,4,5-trioctyloxybenzoyl)-hydrazide. ^{1}H NMR: (300 MHz, $CDCl_3$), (ppm, from TMS): δ=10.35 (s, 2H), 9.15 (s, 2H), 7.04 (s, 4H), 4.00–3.88 (m, 12H), 1.76–1.67 (m, 12H), 1.42–1.28 (m, 60H), 0.89 (t, 18H, J=6.5Hz). FTIR: ν=3213, 2957, 2926, 2856, 1692, 1629, 1582, 1468, 1427, 1386, 1336, 1231, 1218, 1115, 1007, 957, 858, 782, 750, 722, 601 cm^{-1}. Anal. Calcd (%) for $C_{64}H_{110}N_4O_{10}$: C, 70.16; H, 10.12; N, 5.11. Found: C, 70.35; H, 10.09; N, 4.85.

4.1.7. Oxalyl acid *N*′,*N*′-di(3,4,5-tridecyloxybenzoyl)-hydrazide. ^{1}H NMR: (300 MHz, $CDCl_3$), (ppm, from TMS): δ=10.31 (s, 2H), 9.08 (s, 2H), 7.04 (s, 4H), 4.02–3.91 (m, 12H), 1.77–1.68 (m, 12H), 1.43–1.26 (m, 84H), 0.86 (t, 18H, J=6.6 Hz). FTIR: ν=3233, 3013, 2955, 2924, 2854, 1693, 1630, 1583, 1487, 1468, 1428, 1385, 1338, 1234, 1211, 1116, 1001, 987, 932, 857, 782, 751, 721, 601 cm^{-1}. Anal. Calcd (%) for $C_{76}H_{134}N_4O_{10}$: C, 72.22; H, 10.69; N, 4.43. Found: C, 72.23; H, 10.92; N, 4.50.

4.1.8. 2,2′-Bis(3,4,5-tripropyloxyphenyl)-bi-1,3,4-oxadiazole. ^{1}H NMR: (300 MHz, $CDCl_3$), (ppm, from TMS): 7.42 (s, 4H), 4.09–4.04 (m, 12H), 1.92–1.79 (m, 12H), 1.12–1.04 (m, 18H). FTIR: ν=2966, 2937, 2876, 1591, 1550, 1494, 1474, 1434, 1389, 1355, 1344, 1315, 1306, 1276, 1231, 1154, 1128, 1099, 1061, 1023, 997, 954, 934, 915, 877, 845, 831, 813, 766, 728, 671, 614, 594 cm^{-1}. Anal. Calcd for $C_{34}H_{46}N_4O_8$: C, 63.93; H, 7.26; N, 8.77. Found: C, 63.71; H, 7.19; N, 8.71.

4.1.9. 2,2′-Bis(3,4,5-tributyloxyphenyl)-bi-1,3,4-oxadiazole. ^{1}H NMR: (300 MHz, $CDCl_3$), (ppm, from TMS): 7.41 (s, 4H), 4.12–4.06 (m, 12H), 1.90–1.74 (m, 12H), 1.57–1.50 (m, 12H), 1.03–0.96 (m, 18H). FTIR: ν=3435, 2956, 2933, 2872, 1593, 1545, 1492, 1465, 1437, 1382, 1349, 1306, 1272, 1238, 1133, 1116, 1066, 1025, 996, 955, 937, 887, 848, 837, 793, 728, 671, 598 cm^{-1}. Anal. Calcd for $C_{40}H_{58}N_4O_8$: C, 66.46; H, 8.09; N, 7.75. Found: C, 66.58; H, 8.10; N, 7.96.

4.1.10. 2,2′-Bis(3,4,5-tripentyloxyphenyl)-bi-1,3,4-oxadiazole. ^{1}H NMR: (300 MHz, $CDCl_3$), (ppm, from TMS): 7.41 (s, 4H), 4.12–4.05 (m, 12H), 1.90–1.76 (m, 12H), 1.55–1.38 (m, 24H), 0.98–0.92 (m, 18H). FTIR: ν=2953, 2863, 1590, 1551, 1495, 1473, 1433, 1382, 1351, 1316, 1276, 1243, 1232, 1151, 1133, 1118, 1071, 1050, 1021, 991, 955, 929, 913, 893, 867, 841, 806, 779, 728, 671, 599 cm^{-1}. Anal. Calcd for $C_{46}H_{70}N_4O_8$: C, 68.46; H, 8.74; N, 6.94. Found: C, 68.61; H, 8.83; N, 7.06. MALDI-TOF MS: *m*/*z*: calcd for : 806.5, found: 806.2.

4.1.11. 2,2′-Bis(3,4,5-trihexyloxyphenyl)-bi-1,3,4-oxadiazole. ^{1}H NMR: (300 MHz, $CDCl_3$), (ppm, from TMS): 7.41 (s, 4H), 4.12–4.05 (m, 12H), 1.91–1.75 (m, 12H), 1.60–1.42 (m, 12H), 1.39–1.32 (m, 24H), 0.95–0.90 (m, 18H). FTIR: ν=2934.12, 2871, 1591, 1549, 1494, 1487, 1441, 1432, 1380, 1352, 1272, 1242, 1133, 1021, 980,

840, 797, 727, 672, 601 cm^{-1}. Anal. Calcd for $C_{52}H_{82}N_4O_8$: C, 70.08; H, 9.27; N, 6.29. Found: C, 70.31; H, 9.39; N, 6.14.

4.1.12. 2,2′-Bis(3,4,5-triheptyloxyphenyl)-bi-1,3,4-oxadiazole. ^1H NMR: (300 MHz, $CDCl_3$), (ppm, from TMS): 7.41 (s, 4H), 4.11–4.05 (m, 12H), 1.91–1.75 (m, 12H), 1.54–1.49 (m, 12H), 1.40–1.32 (m, 36H), 0.92–0.88 (m, 18H). FTIR: ν=2953, 2923, 2870, 2852, 1589, 1549, 1493, 1466, 1430, 1389, 1351, 1305, 1276, 1240, 1193, 1148, 1131, 1117, 1070, 1024, 1006, 964, 954, 954, 936, 881, 842, 812, 773, 727, 672, 597 cm^{-1}. Anal. Calcd for $C_{58}H_{94}N_4O_8$: C, 71.42; H, 9.71; N, 5.74. Found: C, 71.18; H, 9.91; N, 5.40.

4.1.13. 2,2′-Bis(3,4,5-trioctanoxyphenyl)-bi-1,3,4-oxadiazole. ^1H NMR: (300 MHz, $CDCl_3$), (ppm, from TMS): 7.41 (s, 4H), 4.11–4.05 (m, 12H), 1.88–1.76 (m, 12H), 1.52–1.49 (m, 12H), 1.40–1.30 (m, 48H), 0.90–0.88 (m, 18H). FTIR: ν=2923, 2851, 1591, 1549, 1493, 1466, 1432, 1390, 1351, 1277, 1243, 1149, 1130, 1118, 1026, 954, 870, 842, 295, 727, 672, 598 cm^{-1}. Anal. Calcd for $C_{64}H_{106}N_4O_8$: C, 72.55; H, 10.08; N, 5.25. Found: C, 72.73; H,10.14; N, 4.92. MALDI-TOF MS: *m/z*: calcd for : 1058.8, found: 1058.6.

4.1.14. 2,2′-Bis(3,4,5-tridecyloxyphenyl)-bi-1,3,4-oxadiazole. ^1H NMR: (300 MHz, $CDCl_3$), (ppm, from TMS): 7.41 (s, 4H), 4.11–4.05 (m, 12H), 1.89–1.76 (m, 12H), 1.52–1.49 (m, 12H), 1.40–1.28 (m, 72H), 0.91–0.86 (m, 18H). FTIR: ν=2952, 2849, 1589, 1550, 1494, 1468, 1442, 1430, 1387, 1352, 1308, 1276, 1242, 1149, 1131, 1121, 1067, 1047, 1022, 973, 954, 926, 880, 860, 843, 827, 795, 764, 764, 727, 672, 599 cm^{-1}. Anal. Calcd for $C_{76}H_{130}N_4O_8$: C, 74.34; H, 10.67; N, 4.56. Found: C, 74.36; H, 10.57; N, 4.54.

4.1.15. 2,2′-Bis(3,4,5-tritetradecyloxyphenyl)-bi-1,3,4-oxadiazole. ^1H NMR: (300 MHz, $CDCl_3$), (ppm, from TMS): 7.41 (s, 4H), 4.11–4.04 (m, 12H), 1.89–1.75 (m, 12H), 1.53–1.50 (m, 12H), 1.40–1.26 (m, 120H), 0.90–0.86 (m, 18H). FTIR: ν=2920, 2850, 1590, 1547, 1490, 1469, 1434, 1386, 1356, 1315, 1274, 1237, 1147, 1124, 1027, 991, 968, 953, 873, 844, 780, 727, 721, 671, 599 cm^{-1}. Anal. Calcd for $C_{100}H_{178}N_4O_8$: C, 76.77; H, 11.47; N, 3.58. Found: C, 77.13; H, 11.50; N, 3.46.

Acknowledgements

The authors are grateful to the National Science Foundation Committee of China (project no. 50373016), Program for New Century Excellent Talents in Universities of China Ministry of Education, Special Foundation for PhD Program in Universities of China Ministry of Education (project no. 20050183057), and Project 985-Automotive Engineering of Jilin University for their financial support of this work.

Supplementary data

XRD patterns, DSC chart, and photophysical properties of BOXD-T*n*. Supplementary data associated with this article can be found in the online version, at doi:10.1016/j.tet.2007.09.028.

References and notes

1. (a) Reviews Schultz, B.; Bruma, M.; Brehmer, L. *Adv. Mater.* **1997**, *9*, 601; (b) Thelakkat, M.; Schmidt, H.-W. *Polym. Adv. Technol.* **1998**, *9*, 429.
2. Tokuhisa, H.; Era, M.; Tsutsui, T.; Saito, S. *Appl. Phys. Lett.* **1995**, *66*, 3433.
3. (a) Zheng, Y.; Lin, J.; Liang, Y.; Lin, Q.; Yu, Y.; Meng, Q.; Zhou, Y.; Wang, S.; Wang, H.; Zhang, H. *J. Mater. Chem.* **2001**, *11*, 2615; (b) Sano, T.; Nishio, Y.; Hamada, Y.; Takahashi, H.; Usuki, T.; Shibata, K. *J. Mater. Chem.* **2000**, *10*, 157; (c) Noda, T.; Ogawa, H.; Noma, N.; Shirota, Y. *J. Mater. Chem.* **1999**, *9*, 2177; (d) Jiang, X.; Liu, Y.; Tian, H.; Qiu, W.; Song, X.; Zhua, D. *J. Mater. Chem.* **1997**, *7*, 1395; (e) Carella, A.; Castaldo, A.; Centore, R.; Fort, A.; Sirigu, A.; Tuzi, A. *J. Chem. Soc., Perkin Trans. 2* **2002**, 1791; (f) Wang, J.; Wang, R.; Yang, J.; Zheng, Z.; Carducci, M. D.; Cayou, T. *J. Am. Chem. Soc.* **2001**, *123*, 6179.
4. (a) O'Neill, M.; Kelly, S. M. *Adv. Mater.* **2003**, *15*, 1135; (b) van Breemen, A. J. J. M.; Herwig, P. T.; Chlon, C. H. T.; Sweelssen, J.; Schoo, H. F. M.; Setayesh, S.; Hardeman, W. M.; Martin, C. A.; de Leeuw, D. M.; Valeton, J. J. P.; Bastiaansen, C. W. M.; Broer, D. J.; Popa-Merticaru, A. R.; Meskers, S. C. J. *J. Am. Chem. Soc.* **2006**, *128*, 2336.
5. (a) Struijk, C. W.; Sieval, A. B.; Dakhorst, J. E. J.; Kimkes, P.; Koehorst, R. B. M.; Donker, H.; Schaafsma, T. J.; Picken, S. J.; van de Craats, A. M.; Warman, J. M.; Zuilhof, H.; Sudhölter, E. J. R. *J. Am. Chem. Soc.* **2000**, *122*, 11057; (b) Grimsdale, A. C.; Müllen, K. *Angew. Chem., Int. Ed.* **2005**, *44*, 5592.
6. (a) Karamysheva, L. A.; Torgova, S. I.; Agafonova, I. F.; Petrov, V. F. *Liq. Cryst.* **2000**, *27*, 393; (b) Semmler, K. J. K.; Dingemans, T. J.; Samulski, E. T. *Liq. Cryst.* **1998**, *24*, 799; (c) Hetzheim, A.; Wasner, C.; Werner, J.; Kresse, N.; Tschierske, C. *Liq. Cryst.* **2000**, *26*, 885; (d) Tokuhisa, H.; Era, M.; Tsutsui, T. *Adv. Mater.* **1998**, *10*, 404.
7. Kim, B. G.; Kim, S.; Park, S. Y. *Tetrahedron Lett.* **2001**, *42*, 2697.
8. Zhang, Y. D.; Jespersen, K. G.; Kempe, M.; Kornfield, J. A.; Barlow, S.; Kippelen, B.; Marder, S. R. *Langmuir* **2003**, *19*, 6534.
9. (a) Lai, C. K.; Ke, Y. C.; Su, J. C.; Lu, C. S.; Li, W. R. *Liq. Cryst.* **2002**, *29*, 915; (b) Wen, C. R.; Wang, Y. J.; Wang, H. C.; Sheu, H. S.; Lee, G. H.; Lai, C. K. *Chem. Mater.* **2005**, *17*, 1646.
10. Ye, K. Q.; Wang, J.; Sun, H.; Liu, Y.; Mu, Z. C.; Li, F.; Jiang, S. M.; Zhang, J. Y.; Zhang, H. X.; Wang, Y.; Che, C. M. *J. Phys. Chem. B* **2005**, *109*, 8008.